Post-Compensation of Ultra-Wideband Antenna Dispersion Using Microwave Photonic Phase Filters and Its Applications to UWB Systems

Ehsan Hamidi, *Student Member, IEEE*, and Andrew M. Weiner, *Fellow, IEEE*

***Abstract*—We demonstrate experimental post-compensation of ultra-wideband (UWB) antenna dispersion at a receiver front-end by using programmable microwave photonic phase filtering. After the received RF signal is modulated onto an optical carrier, we utilize a hyperfine resolution optical pulse shaper to apply the conjugate of its spectral phase in the optical domain. After optical-to-electronic conversion, this yields an electrical waveform, which is compressed to bandwidth-limited duration. Further we use this technique in two schemes: a radar configuration in which we resolve two close echoes from different paths, which initially interfere and mask each other due to the dispersed response of the antenna link, and a spread-time UWB transmission configuration in which we retrieve and compress a distorted signal received in line-of-sight. To our knowledge, this is the first experimental demonstration of dispersion post-compensation of UWB RF waveforms to approach the ultimate bandwidth-limited resolution, as well as identification of such signals by matched filtering and compression. Our technique is programmable and offers potential to enhance performance in UWB radar and communications.**

***Index Terms*—Antenna dispersion, microwave photonics, radar resolution, ultra-wideband (UWB) systems.**

I. Introduction

INTEREST IN ultra-wideband (UWB) systems has grown rapidly due to appealing features such as high data rate, multiaccess, and low probability of intercept communications. The application of UWB to ranging and radar has also received attention [1]–[3] due to the potential for hyperfine range resolution. However, the efficient use of single-carrier large fractional bandwidth signals that efficiently utilize the ultrawide bandwidth allocated by the Federal Communications Commission (FCC) [4] remains a challenge. Manipulation of large instantaneous bandwidth UWB signals incurs challenges related to generation, transmission, and detection.

Although electronic generation of UWB impulses has been extensively investigated, microwave photonic techniques have demonstrated superior capability for generation of arbitrary UWB waveforms with instantaneous bandwidths beyond that offered by electronic solutions [5]–[11]. Processing of large instantaneous bandwidth UWB signals for detection in a receiver is an even more challenging problem. Correlation schemes are one common approach; however, bandwidths are limited and precise synchronization is required. To date, surface acoustic wave (SAW) technology offers the largest bandwidth for asynchronous real-time processing. However, SAW correlators have been demonstrated only for bandwidths up to 1.1 GHz (30% fractional bandwidth of the 3.63-GHz center frequency), well below the full bandwidths potentially available for UWB, with insertion loss of 23 dB even after accounting for the pulse compression gain [12]. Furthermore, the correlation function for such SAW devices is fixed (not programmable), and further progress is difficult due to shrinking dimensions and increased loss associated with higher center frequencies and larger bandwidth. Digital signal-processing techniques for large instantaneous bandwidth UWB systems are limited by the speed of analog to digital converters (ADCs) [13], [14].

A new approach is to use RF photonic phase filters for asynchronous matched filtering and compression of UWB RF waveforms. In recent experiments in a wired configuration, we demonstrated programmable matched filtering and compression of RF waveforms with up to 15-GHz instantaneous bandwidth [15]. Here, for the first time, we demonstrate the use of programmable RF photonic phase filters for asynchronous matched filtering of UWB signals after line-of-sight wireless transmission. The resultant pulse compression functionality may contribute to enhanced range resolution for radar and enhanced data rates and multiple-access capability for communications.

One of the key limitations in UWB transmission systems [16], particularly in line-of-sight, is signal distortion due to dispersion and frequency dependent transmission. Channel nonuniformity assuming no emission regulation is arising from nonuniform spectral amplitude response of the channel including the receiver and transmitter elements, which determines the effective channel bandwidth. To overcome this limitation, shaping the transmitting signal spectrum has been proposed in [8] and [17]. Dispersion due to the nonlinear RF spectral phase response of the transmitter and/or receiver elements is the focus of our study in this paper. In particular, for large fractional bandwidth signals, the antennas utilized in a wireless link may contribute very large dispersion to the signal [16], [18], [19]. This problem has been theoretically investigated, and optimization of transmit waveforms in order to maximize the received signal energy or peak voltage has been analyzed [20]–[22]. Recently, experiments have been reported in which photonically generated UWB RF waveforms were

Manuscript received November 04, 2008; revised January 20, 2009. First published March 21, 2009; current version published April 08, 2009. This work was supported in part by the National Science Foundation under Grant 0701448.

The authors are with the School of Electrical and Computer Engineering, Purdue University, West Lafayette, IN 47907-2035 USA (e-mail: ehamidi@purdue.edu; amw@purdue.edu).

Digital Object Identifier 10.1109/TMTT.2009.2015126

synthesized in order to successfully precompensate for antenna dispersion [23]–[25]. The application of photonically generated arbitrary waveforms to measure the frequency-dependent delay of broadband antennas has also been demonstrated [26].

In principle, the precompensation technique relies on generation of a transmit signal shaped according to the time-reversed impulse response of the link. However, in point-to-multipoint systems when diversity is present among receivers, e.g., different receive antennas, this technique cannot compensate all the links simultaneously. Furthermore, in the context of wireless communications, when the delay between adjacent symbols is less than the time spread of the impulse response, this technique requires synthesis of a waveform equal to the coherent combination of two or more delayed precompensation waveforms. This adds to the complexity required from the waveform generator and may exceed current capabilities.

Alternately, real-time post-processing to remove dispersion can be performed at the front end of the receiver. This resolves the problems of receiver diversity and waveform generator complexity. Here, by connecting the output of a receiving antenna to a programmable UWB phase filter implemented in photonics, we demonstrate compensation of the dispersion associated with antennas in a line-of-sight wireless link. In addition, we also demonstrate waveform identification functionality through appropriate programming of the phase filter.

The FCC's regulation on UWB emission [4] includes a constraint on full bandwidth peak power, which has been analyzed as a function of repetition rate for various pulse bandwidths [27]. It is shown that for repetition rates less than 187.5 kHz, the full bandwidth peak power constraint dominates the average power spectral density constraint. Therefore, for fixed bandwidth, one may transmit at higher energy at the allowed peak power by utilizing waveforms that are spread in time by application of spectral phase modulation.

On the other hand, in radar systems where high energy pulses are required at low repetition rate, amplification of large fractional bandwidth impulses becomes a bottleneck because of the tradeoff between bandwidth and output swing in RF power amplifiers. In order to increase pulse energy at a fixed peak voltage, bandwidth-limited pulses are commonly replaced by spread-time waveforms, which are spectrally phase modulated, e.g., linear chirp [28]. Conventionally the return signal is correlated with a replica of the transmit signal to obtain compression and realize the ultimate range resolution. However, this scheme requires accurate timing between received waveforms and reference signals and must be performed in multiple shots or in multichannel processors [28] in the absence of prior knowledge of return signal delay. These problems are particularly difficult when the bandwidths are very large. A different solution is to use a real-time phase filter, which cancels the spectral phase of the waveform. This compresses the waveform to the bandwidth limit, which can be used to improve signal-to-noise ratio and better resolve closely spaced return signals. In this context, we further demonstrate compression of arbitrary waveforms by simultaneously phase compensating the waveform itself and dispersion compensating the wireless link.

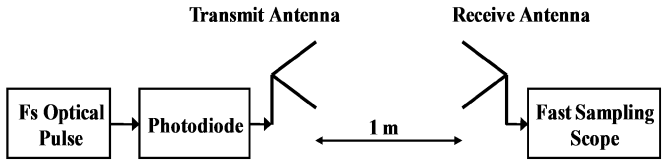

Fig. 1. Antenna link configuration.

II. Experiment

A. Antenna Link Time-Domain Response

Fig. 1 shows the configuration of our pulsed wireless transmission experiments. We use two ridged TEM horn antennas (Dorado International GH1-12N) with a specified bandwidth of 1–12 GHz in line-of-sight separated by about 1 m. The distance of 1 m was chosen to satisfy the far-field constraint at a frequency of 1 GHz. We choose highly directional antennas to avoid multipath interference and focus on the line-of-sight link response. Hence, the received waveform will be distorted mainly from the response of our antennas, and not the multipath effect. We note that although a ridged TEM horn antenna is not as highly dispersive as other UWB antennas such as spirals, the amount of dispersion suffices for a proof-of-concept demonstration of the improvement offered by dispersion compensation.

A photodiode with a 3-dB bandwidth of 22 GHz is driven by a mode-locked laser and its output drives the transmit antenna. The receive antenna is connected to a 26-GHz bandwidth sampling scope. Similar to [23], we obtain the impulse response of the antenna link by exciting the transmit antenna with a 30-ps pulse (410-mV peak voltage) from the photodiode [see inset of Fig. 2(a)]. The measured time-domain response is shown in Fig. 2(a). The short input pulse is obviously dispersed and the received waveform shows clear oscillations over roughly 4 ns. The received waveform is down-chirped with the low-frequency components near the antenna low cutoff frequency of 900 MHz occurring roughly 4 ns after the high-frequency oscillations at the leading edge of the waveform. Since the spectral content of the exciting pulse is much broader than the antenna frequency response, we can simply assume the time-domain response in Fig. 2(a) as the link impulse response. Through Fourier transform, we extract the spectral amplitude (normalized) and phase of the link response, which are shown in Fig. 2(b).

The spectral amplitude of the link frequency response decreases above 1 GHz. This can be explained by the Friis transmission equation [29]

$$P_r = G_t G_r \left(\frac{v}{4\pi f R}\right)^2 P_t \tag{1}$$

where P_r and P_t are receive and transmit powers, G_r and G_t are receive and transmit antenna gains, v is the speed of light in the medium, f is frequency, and R is the distance between antennas. Hence, we can write the antenna link spectral amplitude response as

$$|H_L(\omega)| = G_t(\omega) G_r(\omega) \left(\frac{v}{2\omega R}\right)^2 \tag{2}$$

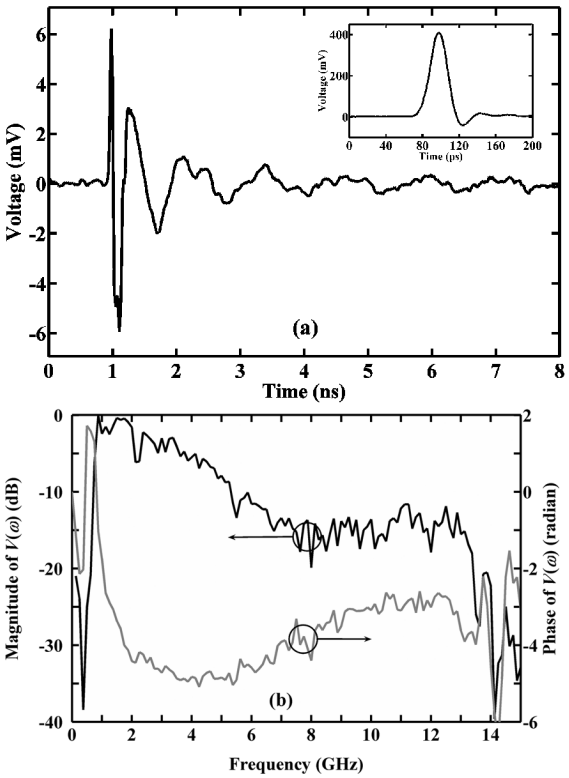

Fig. 2. (a) Ridged-horn antenna link measured time-domain response. The 30-ps driving pulse is shown in the inset. (b) The antenna link frequency response, amplitude (normalized), and phase extracted from the time-domain response.

Since the received power is inversely proportional to frequency squared, the spectral amplitude drops by 20 dB per decade even if the antenna gains are frequency independent. The spectral phase in Fig. 2(b) is plotted after subtraction of the linear part of phase. The subtraction of the linear part of the phase is relevant, as it represents only a constant delay.

B. Experimental Setup

A schematic of our experimental setup is shown in Fig. 3. The core of our setup is a microwave photonic filter, first demonstrated in [30], which is based on optical frequency-domain filtering combined with optical to electrical (O/E) conversion to implement programmable microwave photonic phase filters. The optical frequency-domain filtering is based on Fourier transform pulse shaping [31], which has been extended to hyperfine (about 600 MHz) spectral resolution through the use of a virtually imaged phased array as a spectral disperser [32].

In this technique, RF frequencies are up-converted to optical frequencies, which are then spread out spatially by a spectral disperser and manipulated independently and in parallel through a spatial light modulator. In principle, this enables spectral amplitude and phase control; here we program the spatial light modulator for a phase-only response. Hence, the phase filter imposed onto the optical spectrum is directly mapped onto a microwave phase filter at the output. As a result, a user-defined frequency-domain microwave phase filter is implemented photonically that provides essentially programmable arbitrary phase filter response over an RF band from dc to 20 GHz with about

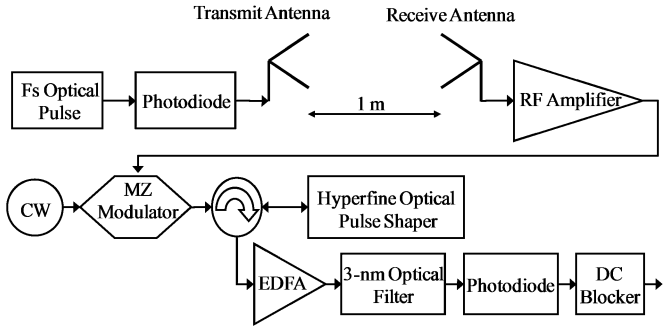

Fig. 3. Experimental setup. The wireless link is followed by an RF amplifier and the microwave photonic phase filter.

600-MHz spectral resolution. The minimum achievable spectral resolution is essentially limited by a spectral disperser. The minimum spectral resolution of a pulse shaper determines the maximum time aperture over which a waveform may be manipulated. A spectral resolution of 600 MHz corresponds to a time aperture of about 730 ps. For more details on such phase filtering, please refer to [15] and [30].

In this setup, a tunable laser with linewidth below 0.1 pm centered at 1550.17 nm is input to a Mach–Zehnder (MZ) intensity modulator with an electrical 3-dB bandwidth of 30 GHz and a minimum transmission voltage V_π of about 4.75 V. The modulator is driven with a broadband RF amplifier (30-dB gain with bandwidth of 0.1–18 GHz) fed by the RF waveform received via the receive horn antenna. The MZ modulator transfers the RF signal into the optical domain as a double-sideband modulation about the optical carrier. The resulting double-sideband modulated signal is input into an optical pulse shaper.

The output of the hyperfine optical pulse shaper is applied to an erbium-doped fiber amplifier. After amplification in an erbium-doped fiber amplifier, the optical signal passes through a 3-nm optical filter to reduce its amplified spontaneous emission. The spectrally-filtered optical signal is then down-converted to baseband via a photodiode with an electrical 3-dB bandwidth of 22 GHz. Since a photodiode maps optical intensity to an electrical signal, the resulting voltage signal is required to be a positive-definite quantity. The corresponding nonzero dc level is removed by a dc blocker. The resultant microwave signal is measured by a fast sampling scope.

The Fourier transform pulse shaper passes both the carrier and both sidebands of the modulated optical signal. By programming the spatial light modulator, a filter with an arbitrary spectral phase can be synthesized and imposed on the optical signal. After O/E conversion, the relation between input and output electrical signals is given by

$$V_o(\omega) = H_F(\omega)V_i(\omega) \tag{3}$$

where $H_{\rm F}(\omega)$ is the microwave photonic filter frequency response, and $V_{\rm i}(\omega)$ and $V_{\rm o}(\omega)$ are the Fourier transforms of input and output electrical signals. For practical signals which are real, one sideband is a complex-conjugate of the other. Thus, in our apparatus, optical phase filters are programmed with complex-conjugate symmetry about the optical carrier frequency. In order to program the microwave photonic filter as a phase-only

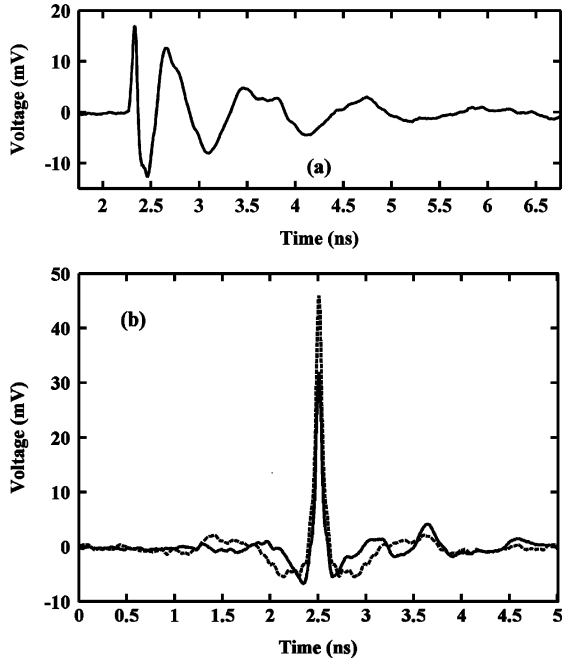

Fig. 4. (a) Output electrical waveform when the pulse shaper is quiescent. (b) Output dispersion compensated electrical waveform after the phase filter is applied, and calculated dispersion-compensated electrical waveform by an ideal photonic phase filter in solid and dashed lines, respectively.

filter, we first extract the spectrum of the output dispersed electrical waveform when the pulse shaper is quiescent, i.e., no spectral phase is added, by taking Fourier transform of the measured output waveform. By imposing the opposite of the output dispersed waveform's spectral phase onto the corresponding optical signal spectrum, the envelope of the optical carrier electric field is compressed to its transform-limited duration. This results after O/E conversion in an electrical pulse that is compressed to a bandwidth-limited duration. In other words, we have $H_{\mathrm{F}}(\omega) = \exp\{-\mathrm{j} < V_{\mathrm{i}}(\omega)\}$, which results in an output electrical signal with spectrum

$$V_o(\omega) = e^{-j\angle V_i(\omega)} V_i(\omega) = |V_i(\omega)|. \tag{4}$$

III. Experimental Results

A. Antenna Dispersion Compensation

The results of antenna link dispersion compensation are shown in Fig. 4, where voltage profiles after the dc blocker of Fig. 3 are plotted. Fig. 4(a) shows the output waveform when the pulse shaper is quiescent. The output waveform after the microwave photonic filter when no spectral phase is added is almost the same as the received dispersed waveform in Fig. 2(a). The spectral phase of the waveform in Fig. 2(a) is then extracted via fast Fourier transform (FFT), and the spatial light modulator in the pulse shaper is programmed for equal, but opposite, spectral phase. Mathematically we have $H_{\mathrm{F}}(\omega) = \exp\{-\mathrm{j} < H_{\mathrm{L}}(\omega)\}$, which results in

$$V_o(\omega) = e^{-j\angle H_L(\omega)} H_L(\omega) V_i(\omega) = |H_L(\omega)| V_i(\omega). \tag{5}$$

Assuming an input bandwidth limited pulse with a bandwidth larger than the link bandwidth, the output signal $V_{\mathrm{o}}(\omega)$ becomes proportional to $|H_{\mathrm{L}}(\omega)|$ with a constant factor. Fig. 4(b) shows the compressed electrical waveform at the output after the conjugate spectral phase is applied through the microwave photonic filter in a solid line. As we expect, the received waveform after dispersion compensation is highly compressed.

The compressed voltage pulse has a duration of 65-ps full width at half maximum (FWHM), which is very close to the bandwidth limit. The residual oscillation around 3.6 ns is due to the fact that our microwave photonic filter has a temporal window less than 1 ns, as mentioned in Section II; wings of the received waveform corresponding to time spreads greater than the phase filter's time aperture cannot be fully dispersion compensated. This limitation also results in asymmetry in the dispersion-compensated waveform. The RF peak power gain is 5.52 dB.

Assuming an ideal photonic phase filter with no spectral resolution or time aperture limits, and setting the spectral phase of the waveform in Fig. 4(a) to zero, we can calculate the ideal dispersion-compensated waveform. The result is shown by a dashed line in Fig. 4(b). The ideal FWHM pulse duration and peak power gain are calculated to be 64 ps and 8.67 dB, respectively. We attribute the slight discrepancy between our experimental and calculated results to abrupt phase changes between adjacent spatial light modulator pixels, which result in diffraction and excess loss at corresponding frequencies. This effect is related to finite spectral resolution and has been investigated recently, for example, in line-by-line pulse shaping [32]. This loss is dependent on the rate of phase change across pixels and is, therefore, waveform and frequency dependent. The difference in peak power gain is due to the fact that the time aperture of the filter is insufficient to fully capture the energy of the dispersed waveform at the correlation point. Nevertheless, our measurements show that the phase of the compressed pulse is corrected with a high degree of precision.

Similar to [23], it is interesting to consider metrics that can be used to quantify how well a signal is dispersion compensated and compressed. We define the sidelobe level of a signal as the ratio of the normalized power of the sidelobes to that of the main lobe in the dispersion compensated signal

$$S = 10\log_{10}\frac{V_n^2}{V_p^2}\ (\mathrm{dB}) \tag{6}$$

where V_n is the voltage magnitude of the nth sidelobe and V_{p} is the voltage magnitude of the main peak.

Fig. 5 shows the corresponding instantaneous power of the waveforms in Fig. 4. The power plots are normalized to their peak power, and the sidelobes are indexed with respect to the main peak. We observe when the pulse shaper is quiescent, the output waveform has a FWHM of 372 ps in terms of power, however, when the antenna link is dispersion-compensated,the FWHM becomes 47 ps, which is in excellent agreement with the ideal dispersion-compensated waveform's FWHM of 46 ps. A summary of the sidelobe levels with respect to the main peak for the antenna link impulse response, the dispersion-compensated response, and the ideal dispersion-compensated response is given in Table I.

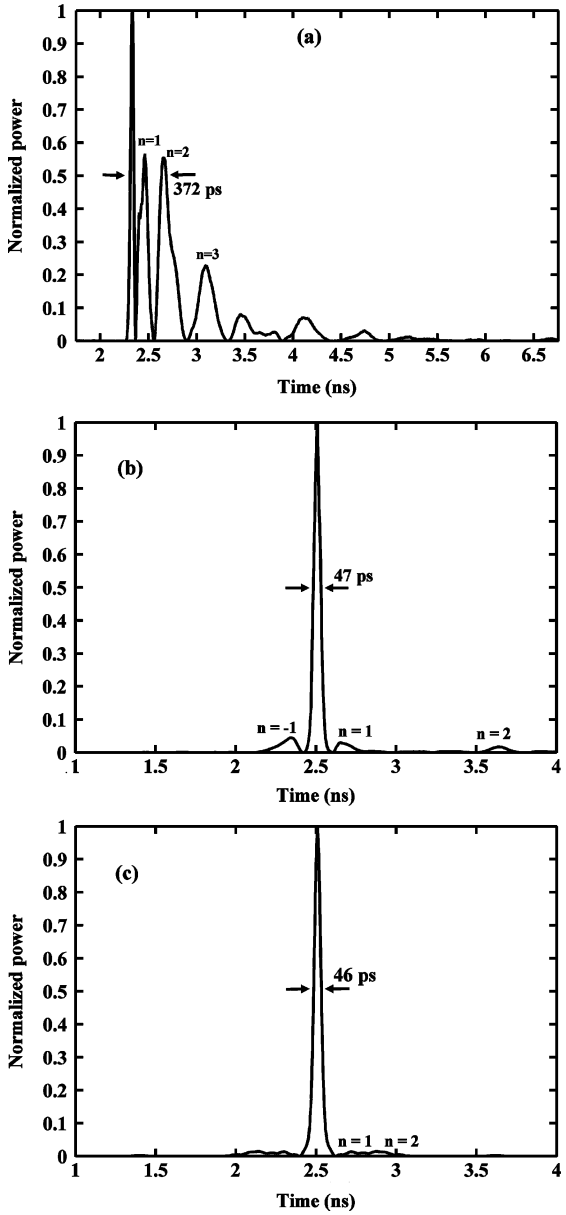

Fig. 5. Comparison of normalized power for: (a) the antenna link impulse response. (b) Measured dispersion-compensated waveform. (c) Calculated dispersion-compensated waveform.

The main sidelobe level from the dispersion-compensated waveform to the antenna link response is reduced from −2.47 to −13.46 dB (11-dB suppression, compared to 7.8-dB suppression in [23]), while calculation predicts up to 16-dB sidelobe suppression for dispersion compensation by an ideal photonic phase filter.

B. Approaching UWB Radar Ultimate Range Resolution

Fig. 6 shows our experimental setup, which mimics a simplified radar configuration. There are two effective propagation paths: line-of-sight and reflection from a target. The centers of the antennas' apertures are separated by about 95.5 cm, and they are tilted upward in order to obtain two paths with equal transmission amplitude. Here we use a metal plate as a target, which is placed 19 cm away from the line-of-sight path. The plate is

TABLE I
COMPARISON OF SIDELOBE LEVELS IN THE RECEIVED WAVEFORM FOR LINK IMPULSE RESPONSE AND DISPERSION COMPENSATED WAVEFORM

Waveform	Sidelobe Index	Location (ps)	Sidelobe Level (dB)
Link Response Fig. 5 (a)	$n = 1$	132	-2.47
	$n = 2$	328	-2.55
	$n = 3$	766	-6.40
	$n = 4$	1140	-10.91
	$n = 5$	1790	-11.49
Dispersion Compensated Fig. 5 (b)	$n = -1$	-165	-13.46
	$n = 1$	153	-15.24
	$n = 2$	1133	-17.72
Ideally Dispersion Compensated Fig. 5 (c)	$n = -2$	-367	-18.45
	$n = -1$	-209	-18.63
	$n = 1$	209	-18.63
	$n = 2$	367	-18.45

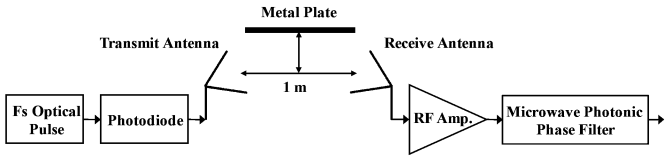

Fig. 6. Radar configuration.

initially positioned relative to the antennas such that the propagating wave from the transmit antenna is incident on the plate in TM polarization, yielding an amplitude reflection coefficient $\Gamma = 1$.

Fig. 7(a) shows the received signal at the receive antenna, which is a combination of two paths. Since the difference in the path lengths corresponds to a time delay much smaller than the antenna's line-of-sight impulse response, the signal contributions from the two paths interfere at the receive antenna. The composite impulse response can be written as

$$h_{\mathrm{ML}}(t) = h_L(t) + a h_L(t-\tau) \tag{7}$$

where $h_{\mathrm{ML}}(t)$ is the overall multipath antenna link impulse response, $h_{\mathrm{L}}(t)$ is the line of sight impulse response, which has a Fourier transform of $H_L(\omega)$, a is a coefficient accounting for the strength of the reflection path with respect to the line-of-sight path, and τ is the delay difference. The overall frequency response is

$$H_{\mathrm{ML}}(\omega) = F\{h_{\mathrm{ML}}(t)\} = H_L(\omega)[1 + a\, e^{-j\omega\tau}]. \tag{8}$$

In Fig. 7(a), large dispersion in the antenna link response makes it difficult or impossible to distinguish the individual signal paths from simple inspection of the received waveform. Signal processing is required to identify the waveform contribution from each path in order to resolve time delays between return signals (related to spatial distances between targets). Instead here we utilize spectral phase filtering to remove undesired dispersion from the antenna link. This compresses the dispersed waveforms from different paths back to bandwidth-limited pulses, which may be resolved at much smaller time off-

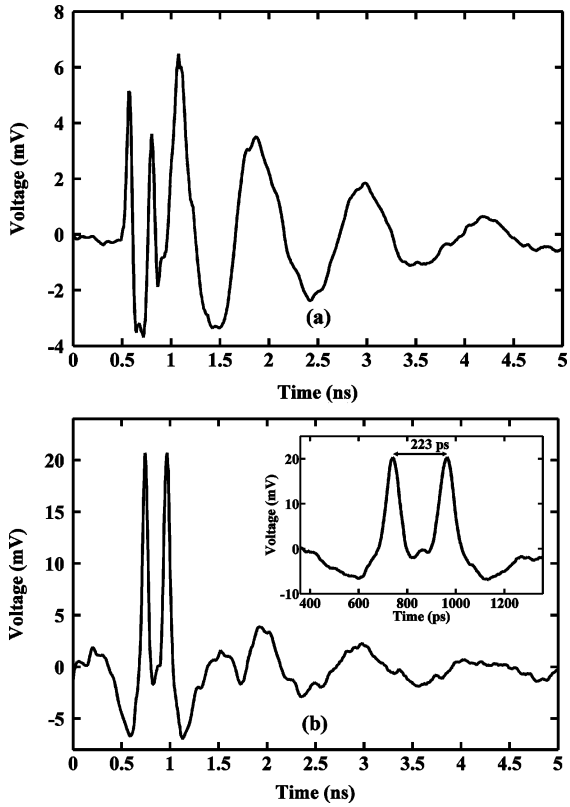

Fig. 7. (a) Radar link response with TM reflection without the phase filter. (b) Radar link response after applying the dispersion compensating filter. Magnified view of two highly resolved pulses is shown in the inset.

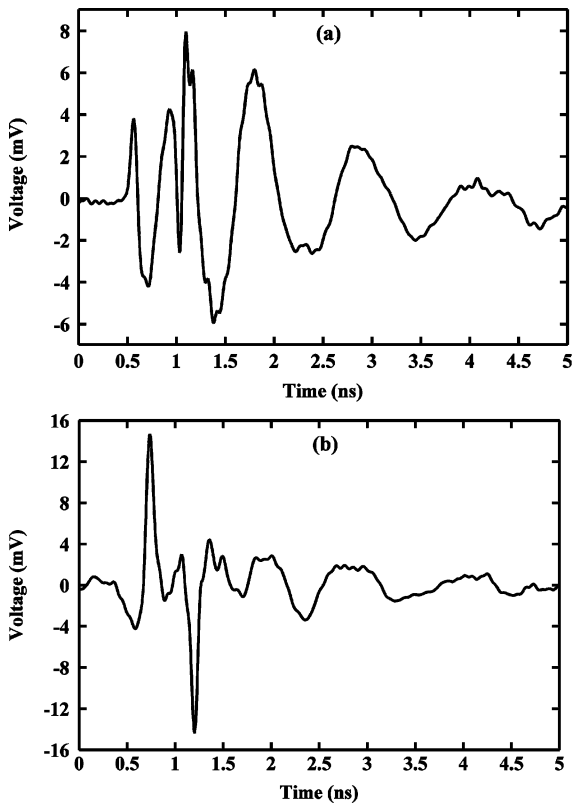

Fig. 8. (a) Radar link response with TE reflection without the phase filter. (b) Radar link response after applying the dispersion compensating filter.

sets. The compressed impulse response of the composite link $h_{\mathrm{CML}}(t)$ may be written

$$h_{\mathrm{CML}}(t) = F^{-1}\{e^{-j\angle H_L(\omega)} H_{\mathrm{ML}}(\omega)\} = h_{\mathrm{CL}}(t) + a h_{\mathrm{CL}}(t-\tau) \tag{9}$$

where $h_{\mathrm{CL}}(t)$ is the compressed impulse response of the line-of-sight antenna link given by

$$h_{\mathrm{CL}}(t) = F^{-1}\{|H_L(\omega)|\}. \tag{10}$$

We note that this technique requires arbitrary phase filters, the design and implementation of which has in the past remained essentially unexploited in the microwave filter design area, particularly for UWB applications.

Fig. 7(b) demonstrates the received signal after dispersion compensation via the programmable microwave photonic phase filter. Now two distinct pulses are clearly resolved, with separation of about 223 ps. A magnified view is shown in the inset. Compared to Fig. 7(a), ringing due to dispersion is significantly suppressed. The polarity of the two pulses is the same, consistent with the TM reflection coefficient equal to one.

The difference between the line-of-sight and reflection paths lengths calculated from the geometry in Fig. 6 is 242 ps, which is in reasonable agreement with the measured 223-ps delay. The slight difference between experiment and calculation arises from referencing our geometrical measurement to the center of the antenna apertures, which apparently does not exactly represent the wave propagation path.

We performed a similar experiment with the apparatus repositioned such that the wave incident on the metal plate is in TE polarization, which has amplitude reflection coefficient equal to -1 ($\Gamma = -1$). Here the centers of the antenna apertures are separated by about 92 cm and the metal plate is placed 26 cm away from the line-of-sight. Fig. 8(a) shows the received signal arising from the combination of the two paths without dispersion compensation. Fig. 8(b) shows the received signal after dispersion compensation via the programmable microwave photonic phase filter. We observe two highly resolved pulses separated by about 490 ps. The polarities of the two pulses are opposite, as expected for TE reflection.

Summarizing the results of this section: we have demonstrated pulse compression over UWB bandwidths, yielding distance resolution proportional to the bandwidth-limited pulse duration. This significantly improves on results without dispersion compensation, where resolution is significantly degraded.

C. Simultaneous Dispersion Compensation and Compression of Spread-Time Waveforms

As mentioned in Section I, the application of UWB spread-time waveforms instead of monopulses may be used to enhance transmit energy from a peak voltage limited transmitter, although utilizing a phase filter to realize pulse compression becomes necessary. Spread-time waveforms may also be employed in UWB wireless communication, for example, for purposes of multiaccess [34], [35].

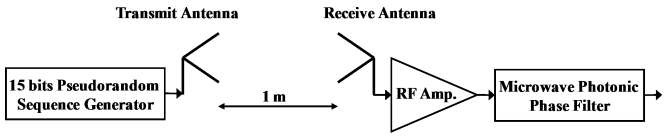

Fig. 9. Experimental setup. 15-bit pseudorandom sequence is generated by Agilent N4901 SerialBERT and transmitted via the wireless link followed by an RF amplifier and the microwave photonic phase filter.

Here we utilize the programmable microwave photonic phase filter both to dispersion compensate the antenna link and simultaneously to compress a specific spread-time waveform. This is achieved by programming the filter to apply the conjugate of the sum of the antenna link spectral phase and the spread-time waveform spectral phase. Hence, by transmitting the spread-time waveform from the transmit antenna, we will obtain a compressed pulse at the output of the microwave photonic phase filter corresponding to each path from the transmit antenna to the receive antenna. Compression of the spread-time waveform at the receiver should also provide gain in RF peak power and improve the signal-to-noise ratio.

Fig. 9 shows the experimental setup, which is similar to the line-of-sight setup of Fig. 3, but with a pattern generator providing the input electrical signal. Here we use the pattern generator from an Agilent N4901B SerialBERT, which we program to generate a periodically repeating pseudorandom sequence of 15-bit length (000100110101111) at 13.5 Gb/s.

Fig. 10(a) shows two cycles of the pattern generator output. The waveform observed at the receive antenna is shown by a solid line in Fig. 10(b). The dashed line shows the simulation result, calculated by convolving the pattern generator output with the antenna link impulse response

$$V_{\mathrm{RPS}}(\omega) = H_L(\omega) V_{\mathrm{PS}}(\omega) \tag{11}$$

where $V_{\mathrm{PS}}(\omega)$ is the Fourier transform of the input pseudorandom sequence (which can be also expressed in Fourier series), and $V_{\mathrm{RPS}}(\omega)$ is the Fourier transform of the distorted received signal. Clearly the pseudorandom sequence pattern cannot be identified due to the distortion introduced by the antenna link dispersion.

Fig. 10(c) shows the output of the phase filter for two cycles when the pulse shaper is quiescent; the signal is similar to that in Fig. 10(b). The output of the phase filter when it is programmed for dispersion compensation of the antenna link response only can be expressed as

$$V_{\mathrm{CLRPS}}(\omega) = e^{-j\angle H_L(\omega)} V_{\mathrm{RPS}}(\omega) = |H_L(\omega)| V_{\mathrm{PS}}(\omega) \tag{12}$$

where $V_{\mathrm{CLRPS}}(\omega)$ is the Fourier transform of the distorted received signal after compensation of antenna link dispersion. The measured received signal with link dispersion compensation only is shown by a solid line in Fig. 10(d). The ideal dispersion-compensated pseudorandom sequence, assuming an ideal photonic phase filter, is calculated by imposing the opposite of the spectral phase extracted from the waveform in Fig. 2(a) and is shown by a dashed line.

With dispersion compensation, we can now identify the pseudorandom sequence pattern, which is marked in the figure by 0's and 1's for one waveform period. However, the signal remains significantly distorted due to attenuation of the higher RF frequencies, which is expected from the low-pass response of the antenna link evident from Fig. 2(b). The simulation, which includes the frequency-dependent amplitude response of the link through the $|H_{\mathrm{L}}(\omega)|$ factor, is in excellent agreement with the measurement results; this provides evidence that the phase response of the link is well compensated.

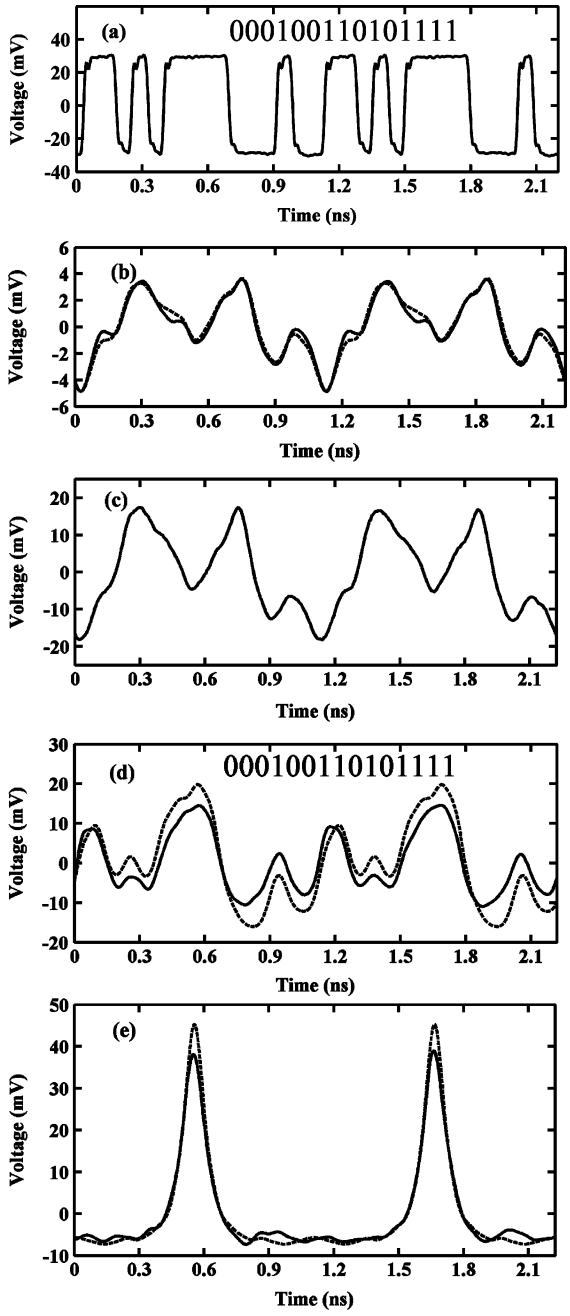

Fig. 10. (a) Generated pseudorandom sequence waveform. (b) Experimental and simulated distorted pseudorandom sequence received through the antenna link in solid and dashed lines, respectively. (c) Output of the microwave photonic filter when the pulse shaper is quiescent. (d) Experimental and simulated retrieved pseudorandom sequence after compensating the antenna link dispersion in solid and dashed lines, respectively. (e) Experimental and simulated received waveform after compensating the antenna link dispersion and conjugate phase filtering the pseudorandom sequence waveform in solid and dashed lines, respectively.

The output of the phase filter after programming the pulse shaper to compensate both the antenna link dispersion and the pseudorandom sequence waveform spectral phase can be written as

$$V_{\mathrm{CLPSRPS}}(\omega) = e^{-j\angle H_L(\omega) - j\angle H_{\mathrm{PS}}(\omega)} V_{\mathrm{RPS}}(\omega) = |H_L(\omega) V_{\mathrm{PS}}(\omega)| \quad (13)$$

The measurement result is shown in Fig. 10(e) via a solid line, while the dashed line shows the simulation result assuming an ideal photonic phase filter programmed according to (13). Clearly each period of the transmitted pseudorandom sequence is compressed to a single, almost bandwidth-limited, pulse. This signifies that compression via spectral phase compensation is robust against distortion arising from frequency-dependent amplitude response. These results, which demonstrate high-quality pulse compression even when superimposing two different frequency dependent phase functions, illustrate the flexibility and accuracy provided by our programmable RF photonic phase filtering approach.

IV. Conclusion

We have experimentally demonstrated post-compensation of the dispersion of a UWB antenna link via programmable microwave phase filters, implemented in photonics. We achieved compression of the time-domain power response of a line-of-sight antenna link from 372-ps duration FWHM to 47 ps, essentially at the bandwidth limit. We have also reported a simple proof-of-concept UWB radar experiment in which such dispersion compensation improves the temporal resolution, allowing clear resolution between return signals separated by 223 ps. Based on the 65-ps compressed signal duration in these experiments, we anticipate a temporal resolution of 32.5 ps, which corresponds to 1-cm path length resolution. We have further presented the application of phase-only matched filtering for simultaneous dispersion compensation and compression of a UWB spread-time transmit waveform. Our technique is fully programmable and may for the first time open up the use of well-known analog signal-processing methods, such as matched filtering, for application to bandwidths in the UWB range and beyond.

We note that the current research utilizes bulk optics pulse-shaping systems, which are likely too expensive for low-cost applications. Here we note that there is significant ongoing research in the integration of optical pulse shaping into semiconductor technology [36], which may, in the future, enable integration of optical processing techniques into compact lower cost devices. On the other hand, in applications such as satellite communications and radar systems, higher cost may be tolerable while achieving much higher performance.

Acknowledgment

The authors would like to thank Senior Research Scientist, D. E. Leaird, Purdue University, West Lafayette, IN, for his helpful technical assistance on this project, and C. Lin, Avanex Corporation, Fremont, CA, for providing Virtually Imaged Phased Array devices.

References

[1] J. Y. Lee and R. A. Scholtz, "Ranging in a dense multipath environment using an UWB radio link," *IEEE J. Sel. Areas Commun.*, vol. 20, no. 9, pp. 1677–1683, Dec. 2002.

[2] J. S. Lee, C. Nguyen, and T. Scullion, "A novel, compact, low-cost, impulse ground-penetrating radar for nondestructive evaluation of pavements," *IEEE Trans. Instrum. Meas.*, vol. 53, no. 6, pp. 1502–1509, Dec. 2004.

[3] R. J. Fontana, L. A. Foster, B. Fair, and D. Wu, "Recent advances in ultrawideband radar and ranging systems," in *IEEE Int. Ultra-Wideband Conf.*, Sep. 2007, pp. 19–25.

[4] "Revision of part 15 of the Commission's rules regarding ultra-wideband transmission systems," FCC, Washington, DC, ET Docket 98-153, adopted Dec. 15, 2004, released Mar. 11, 2005, second report and order and second memorandum opinion and order.

[5] J. Chou, Y. Han, and B. Jalali, "Adaptive RF-photonic arbitrary waveform generator," *IEEE Photon. Technol. Lett.*, vol. 15, no. 4, pp. 581–583, Apr. 2003.

[6] J. D. McKinney, D. S. Seo, D. E. Leaird, and A. M. Weiner, "Photonically assisted generation of arbitrary millimeter-wave and microwave electromagnetic waveforms via direct space-to-time optical pulse shaping," *J. Lightw. Technol.*, vol. 21, no. 12, pp. 3020–3028, Dec. 2003.

[7] I. S. Lin, J. D. McKinney, and A. M. Weiner, "Photonic synthesis of broadband microwave arbitrary waveforms applicable to ultrawideband communication," *IEEE Microw. Wireless Compon. Lett.*, vol. 15, no. 4, pp. 226–228, Apr. 2005.

[8] J. D. McKinney, I. S. Lin, and A. M. Weiner, "Shaping the power spectrum of ultra-wideband radio-frequency signals," *IEEE Trans. Microw. Theory Tech.*, vol. 54, no. 12, pp. 4247–4255, Dec. 2006.

[9] C. Wang and J. P. Yao, "Photonic generation of chirped millimeter-wave pulses based on nonlinear frequency-to-time mapping in a nonlinearly chirped fiber Bragg grating," *IEEE Trans. Microw. Theory Tech.*, vol. 56, no. 2, pp. 542–553, Feb. 2008.

[10] A. Zeitouny, S. Stepanov, O. Levinson, and M. Horowitz, "Optical generation of linearly chirped microwave pulses using fiber Bragg gratings," *IEEE Photon. Technol. Lett.*, vol. 17, no. 3, pp. 660–662, Mar. 2005.

[11] T. Yilmaz, C. M. DePriest, T. Turpin, J. H. Abeles, and P. J. Delfyett, "Toward a photonic arbitrary waveform generator using a modelocked external cavity semiconductor laser," *IEEE Photon. Technol. Lett.*, vol. 14, no. 11, pp. 1608–1610, Nov. 2002.

[12] R. Brocato, J. Skinner, G. Wouters, J. Wendt, E. Heller, and J. Blaich, "Ultrawideband SAW correlator," *IEEE Trans. Ultrason., Ferroelect., Freq. Control*, vol. 53, no. 9, pp. 1554–1556, Sep. 2006.

[13] R. A. Scholtz, D. M. Pozar, and W. Namgoong, "Ultrawideband radio," *EURASIP J. Appl. Signal Process.*, no. 3, pp. 252–272, Mar. 2005.

[14] I. H. Wang and S. I. Liu, "A 1V 5-Bit 5GSample/sec CMOS ADC for UWB receivers," in *Proc. Int. VLSI Design, Automat., Test Symp. Tech. Dig.*, Apr. 2007, pp. 140–143.

[15] E. Hamidi and A. M. Weiner, "Phase-only matched filtering ultrawideband arbitrary microwave waveforms via optical pulse shaping," *J. Lightw. Technol*, vol. 26, no. 15, pp. 2355–2363, Aug. 2008.

[16] J. H. Reed, *An Introduction to Ultra Wideband Communication Systems*. Upper Saddle River, NJ: Prentice-Hall, 2005.

[17] M. Abtahi, M. Mirshafiei, S. LaRochelle, and L. A. Rusch, "All-optical 500 Mb/s UWB transceiver: An experimental demonstration," *J. Lightw. Technol.*, vol. 26, no. 15, pp. 2795–2802, Aug. 2008.

[18] D. Lamensdorf and L. Susman, "Baseband-pulse-antenna techniques," *IEEE Antennas Propag. Mag.*, vol. 36, no. 1, pp. 20–30, Feb. 1994.

[19] A. Shlivinski, E. Heyman, and R. Kastner, "Antenna characterization in the time domain," *IEEE Trans. Antennas Propag.*, vol. 45, no. 7, pp. 1140–1149, Jul. 1997.

[20] D. M. Pozar, R. E. McIntosh, and S. G. Walker, "The optimum feed voltage for a dipole antenna for pulse radiation," *IEEE Trans. Antennas Propag.*, vol. AP-31, no. 4, pp. 563–569, Jul. 1983.

[21] D. M. Pozar, Y.-W. Kang, D. H. Schaubert, and R. E. McIntosh, "Optimization of the transient radiation from a dipole array," *IEEE Trans. Antennas Propag.*, vol. AP-33, no. 1, pp. 69–75, Jan. 1985.

[22] D. M. Pozar, "Waveform optimizations for ultrawideband radio systems," *IEEE Trans. Antennas Propag.*, vol. 51, no. 9, pp. 2335–2345, Sep. 2003.

[23] J. D. McKinney and A. M. Weiner, "Compensation of the effects of antenna dispersion on UWB waveforms via optical pulse-shaping techniques," *IEEE Trans. Microw. Theory Tech.*, vol. 54, no. 4, pp. 1681–1686, Apr. 2006.

[24] A. M. Weiner, J. D. McKinney, and D. Peroulis, "Photonically-synthesized waveforms to combat broadband antenna phase distortions," in *IEEE Int. Microw. Photon. Top. Meeting*, Oct. 2007, pp. 82–83.

[25] J. D. McKinney, D. Peroulis, and A. M. Weiner, "Dispersion limitations of ultra-wideband wireless links and their compensation via photonically enabled arbitrary waveform generation," *IEEE Trans. Microw. Theory Tech.*, vol. 56, no. 3, pp. 710–719, Mar. 2008.
[26] J. D. McKinney, D. Peroulis, and A. M. Weiner, "Time-domain measurement of the frequency-dependent delay of broadband antennas," *IEEE Trans. Antennas Propag.*, vol. 56, no. 1, pp. 39–47, Jan. 2008.
[27] R. J. Fontana and E. A. Richley, "Observations on low data rate, short pulse UWB systems," in *IEEE Int. Ultra-Wideband Conf.*, Sep. 2007, pp. 334–338.
[28] J. D. Taylor, *Ultrawideband Radar Technology*. Boca Raton, FL: CRC, 2001.
[29] D. M. Pozar, *Microwave Engineering*, 3rd ed. New York: Wiley, 2004.
[30] S. Xiao and A. M. Weiner, "Programmable photonic microwave filters with arbitrary ultra-wideband phase response," *IEEE Trans. Microw. Theory Tech.*, vol. 54, no. 11, pp. 4002–4008, Nov. 2006.
[31] A. M. Weiner, "Femtosecond pulse shaping using spatial light modulators," *Rev. Sci. Instrum.*, vol. 71, no. 5, pp. 1929–1960, May 2000.
[32] M. Shirasaki, "Large angular dispersion by a virtually imaged phased array and its application to a wavelength demultiplexer," *Opt. Lett.*, vol. 21, no. 5, pp. 366–368, Mar. 1996.
[33] C.-B. Huang, Z. Jiang, D. E. Leaird, and A. M. Weiner, "The impact of optical comb stability on waveforms generated via spectral line-by-line pulse shaping," *Opt. Exp.*, vol. 14, no. 26, pp. 13164–13176, Dec. 2006.
[34] J. A. Salehi, A. M. Weiner, and J. P. Heritage, "Coherent ultrashort light pulse code-division multiple access communication systems," *J. Lightw. Technol.*, vol. 8, no. 3, pp. 478–491, Mar. 1990.
[35] P. M. Crespo, M. L. Honig, and J. A. Salehi, "Spread-time code-division multiple access," *IEEE Trans. Commun.*, vol. 43, no. 6, pp. 2139–2148, Jun. 1995.
[36] M. J. R. Heck, P. Munoz, B. W. Tilma, E. A. J. M. Bente, Y. Barbarin, Y. S. Oei, R. Notzel, and M. K. Smit, "Design, fabrication and characterization of an InP-based tunable integrated optical pulse shaper," *IEEE J. Quantum Electron.*, vol. 44, no. 4, pp. 370–377, Apr. 2008.

Ehsan Hamidi (S'08) was born in Tehran, Iran, in 1983. He received the B.S. degree in electrical engineering from the Sharif University of Technology, Tehran, Iran, in 2005, and is currently working toward the Ph.D. degree at Purdue University, West Lafayette, IN.

Since 2005, he has been a Research Assistant with the School of Electrical and Computer Engineering, Purdue University. His current research interests include microwave photonics with applications in UWB communication, ultrafast optics, optical pulse shaping, and optical fiber communications.

Mr. Hamidi is a student member of the IEEE Lasers and Electro-Optics Society (LEOS) and the IEEE Communication Society. He has served as a reviewer for the JOURNAL OF LIGHTWAVE TECHNOLOGY.

Andrew M. Weiner (S'84–M'84–SM'91–F'95) received the Sc.D. degree in electrical engineering from the Massachusetts Institute of Technology (MIT), Cambridge, in 1984.

Upon graduation, he joined Bellcore, initially as a Member of Technical Staff, then becoming a Manager of ultrafast optics and optical signal processing research. IN 1992, he joined Purdue University, West Lafayette, IN, where he is currently the Scifres Family Distinguished Professor of Electrical and Computer Engineering. He has authored or coauthored six book chapters and over 200 journal papers. He has authored or coauthored over 350 conference papers, including approximately 80 conference invited talks, and has presented nearly 100 additional invited seminars at university, industry, and government organizations. He has been an associate editor for several journals. He holds ten U.S. patents. His research focuses on ultrafast optics signal processing and applications to high-speed optical communications and UWB wireless. He is especially well known for his pioneering work in the field of femtosecond pulse shaping.

Prof. Weiner is a Fellow of the Optical Society of America (OSA). He is a member of the U.S. National Academy of Engineering. He has served as co-chair of the Conference on Lasers and Electro-optics and the International Conference on Ultrafast Phenomena. He has also served as secretary/treasurer of the IEEE Lasers and Electro-Optics Society (LEOS) and as a vice-president of the International Commission on Optics (ICO). He was the recipient of numerous awards including the Hertz Foundation Doctoral Thesis Prize (1984), the Adolph Lomb Medal of the OSA (1990), the Curtis McGraw Research Award of the American Society of Engineering Education (1997), the International Commission on Optics Prize (1997), and the Alexander von Humboldt Foundation Research Award for Senior U.S. Scientists (2000). He was corecipient of the IEEE LEOS William Streifer Scientific Achievement Award (1999) and the OSA R. W. Wood Prize (2008). He has been recognized by Purdue University with the inaugural Research Excellence Award presented by the Schools of Engineering (2003) and the Provost's Outstanding Graduate Student Mentor Award (2008).